

*Use the template dedic.tex together with the Springer Nature document class SVMono for monograph-type books or SVMult for contributed volumes to style a quotation or a dedication at the very beginning of your book*



# **Foreword**

Place

*Foreword author*



## Preface

Place, Date

*Editors*



## Acknowledgements

Use the template *acknow.tex* together with the document class SVMono (monograph-type books) or SVMult (edited books) if you prefer to set your acknowledgement section as a separate chapter instead of including it as last part of your preface.



# Contents

<b>1</b>	<b>Sample title for chapter 1</b>	1
	U. N. Owen and U. N. Owena	
<b>2</b>	<b>Blood flow in the beating heart: Coupling fluid dynamics to reduced wall and circulation models for data-driven cardiac FSI</b>	3
	Marc Hirschvogel, Mia Bonini, Maximilian Balmus, David Nordsletten	
	<b>Glossary</b>	17
	<b>Index</b>	19



## **List of Contributors**



## **Acronyms**

Use the template *acronym.tex* together with the document class SVMono (monograph-type books) or SVMult (edited books) to style your list(s) of abbreviations or symbols.

Lists of abbreviations, symbols and the like are easily formatted with the help of the Springer Nature enhanced description environment.

ABC      Spelled-out abbreviation and definition

BABI      Spelled-out abbreviation and definition

CABR      Spelled-out abbreviation and definition



# **Chapter 1**

## **Sample title for chapter 1**

U. N. Owen and U. N. Owena

### **Abstract**

Lorem ipsum dolor sit amet, consectetuer adipiscing elit. Ut purus elit, vestibulum ut, placerat ac, adipiscing vitae, felis. Curabitur dictum gravida mauris. Nam arcu libero, nonummy eget, consectetuer id, vulputate a, magna. Donec vehicula augue eu neque. Pellentesque habitant morbi tristique senectus et netus et malesuada fames ac turpis egestas. Mauris ut leo. Cras viverra metus rhoncus sem. Nulla et lectus vestibulum urna fringilla ultrices. Phasellus eu tellus sit amet tortor gravida placerat. Integer sapien est, iaculis in, pretium quis, viverra ac, nunc. Praesent eget sem vel leo ultrices bibendum. Aenean faucibus. Morbi dolor nulla, malesuada eu, pulvinar at, mollis ac, nulla. Curabitur auctor semper nulla. Donec varius orci eget risus. Duis nibh mi, congue eu, accumsan eleifend, sagittis quis, diam. Duis eget orci sit amet orci dignissim rutrum.

### **Introduction**

Sample references Alnæs et al. (2015); Baratta et al. (2023). Source code for this book is found at [github.com/meg-simula/2024-fenics-proceedings](https://github.com/meg-simula/2024-fenics-proceedings)

**Acknowledgements** Please including any acknowledgements, including funding, here.

---

U. N. Owen e-mail: [email@place.edu](mailto:email@place.edu)  
Institution

## References

- Alnæs MS, Blechta J, Hake JE, Johansson A, Kehlet B, Logg A, Richardson C, Ring J, Rognes ME, Wells GN (2015) The fenics project version 1.5. Archive of Numerical Software 3
- Baratta IA, Dean JP, Dokken JS, Habera M, Hale JS, Richardson CN, Rognes ME, Scroggs MW, Sime N, Wells GN (2023) DOLFINx: The next generation FEniCS problem solving environment. doi:10.5281/zenodo.10447666, URL <https://doi.org/10.5281/zenodo.10447666>

## Chapter 2

# Blood flow in the beating heart: Coupling fluid dynamics to reduced wall and circulation models for data-driven cardiac FSI

Marc Hirschvogel, Mia Bonini, Maximilian Balmus, David Nordsletten

**Abstract** We present a fluid-reduced-solid interaction (FrSI) approach suitable for modeling blood flow in the beating left heart. The method uses image-derived model data to construct a suitable boundary motion space, enhanced by a reduced solid mechanics wall model to enable adaptive fluid motion. The method combines the efficiency of fluid dynamics models with features from full FSI approaches, uniquely integrating motion data to predict cardiac hemodynamics over a full heart cycle. The approach is presented for a patient-specific left heart model coupled to a lumped circulatory system, showing physiological flow behavior and pressure-volume relations.

## Introduction

Computational fluid dynamics (CFD) provides a valuable tool to predict blood flow in the cardiovascular system Schwarz et al. (2023). Models of blood flow in the heart have become relevant to predict various cardiovascular conditions, where motion states from imaging are used Bonini et al. (2022); Zingaro et al. (2023); García-Villalba et al. (2021) or even fully-coupled fluid-solid interaction (FSI) models are employed Nordsletten et al. (2011); McCormick et al. (2011). However, prescribed cavity motion reduces the model's ability to adapt under varying loads, and full FSI models are complex, computationally demanding, and difficult to constrain (uncertain boundary conditions and sparse patient data for reliable geometry reconstruction). The fluid-reduced-solid interaction (FrSI) method closes the gap between model complexity and efficiency. This is a data-informed model reduction approach, particularly suited for cardiac FSI Hirschvogel et al. (2024). The method combines physics- with projection-based model reduction techniques that

---

Marc Hirschvogel e-mail: [marc.hirschvogel@polimi.it](mailto:marc.hirschvogel@polimi.it)  
MOX, Dipartimento di Matematica, Politecnico di Milano, Milan, Italy

leverage Proper Orthogonal Decomposition (POD) modes derived from imaging (or some high-fidelity model) to build a reduced-order model (ROM), combined with a structural model of the ventricular wall defined on a 2D manifold. In this contribution, we show the FrSI method's applicability to a complex, patient-specific left heart model, with a particular focus on monolithic solver implementations in FEniCSx Alnæs et al. (2015); Baratta et al. (2023). This method encompasses the implementation of an Arbitrary Lagrangian-Eulerian (ALE) fluid mechanics problem subject to non-local constraints (Galerkin ROM, 3D-0D coupling to lumped circulation models). The solver and preconditioning aspects of this model and other fluid dynamics problems under non-local boundary conditions have been introduced in Hirschvogel et al. (2025).

## Methods

The fluid-reduced-solid interaction (FrSI) problem of a 3D left heart model (atrium, ventricle, aortic outflow tract) along with the underlying data sources is depicted in Fig. 2.1. In particular, domain and motion data are retrieved from time-resolved dynamic computed tomography (CT), which are subsequently mapped to a finite element mesh in order to generate a discrete space of modes using POD Rathinam and Petzold (2003). The model is further coupled to a closed-loop systemic, pulmonary, and coronary circulation system Hirschvogel et al. (2017); Arthurs et al. (2016) in order to provide physiologically meaningful cardiovascular loads to the 3D model.

### Preprocessing of patient data

The FrSI approach relies on external data sourced either from some high-dimensional model or from patient-specific imaging data. Here, we build a patient-specific model of the left heart by segmenting a dynamic cardiac CT data set using 3D Slicer Kikinis et al. (2014), cf. Fig. 2.1A. Subsequently, a diastolic frame is meshed with SimModeler Simmetrix Inc. (2023), and a motion tracking algorithm is used to extract the wall velocities at each frame and map them to the finite element mesh (with velocity degree of freedom space of size  $n_v$ ). Thereafter, the wall velocity data for  $m = 19$  frames is collected into a snapshot matrix  $\hat{\mathbf{S}} \in \mathbb{R}^{n_v \times m}$ , and the eigenvalue problem

$$(\hat{\mathbf{S}}^T \hat{\mathbf{S}}) \boldsymbol{\psi}_i = \lambda_i \boldsymbol{\psi}_i, \quad i = 1, \dots, m, \quad (2.1)$$

is solved, with eigenvalues  $\lambda$  and eigenvectors  $\boldsymbol{\psi} \in \mathbb{R}^m$ . The first  $r_v$  POD modes  $\boldsymbol{\phi} \in \mathbb{R}^{n_v}$  then can be computed as follows:

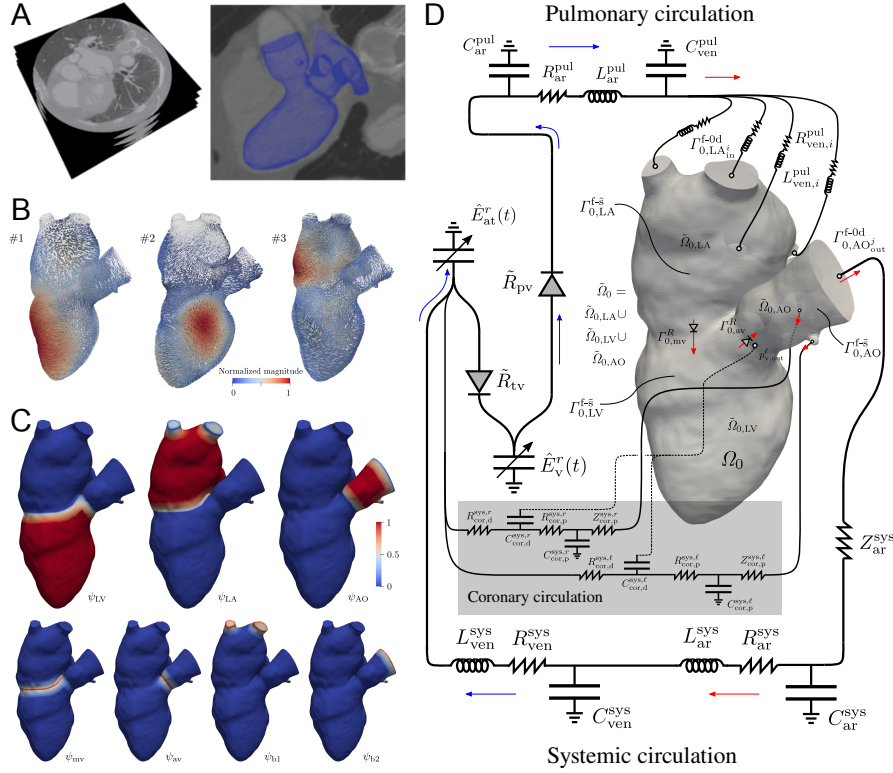


Fig. 2.1: **A.** Dynamic cardiac computed tomography (CT) images with contrast and dynamic segmentation of left heart lumen for subsequent finite element mesh generation, motion tracking of deformation over the heart cycle. **B.** Principal component analysis by means of Proper Orthogonal Decomposition (POD) of wall motion space. The first three most dominant POD modes are shown (10 are used). **C.** Partition of unity fields for regional decomposition of POD space: Atrium, ventricle, and aortic outflow tract—as well as their junctions and truncations around the in-/outflows—can exhibit independent kinematics. **D.** 3D-0D coupled FrSI model of the left heart.

$$\phi_j = \frac{1}{\sqrt{\lambda_j}} \hat{\mathbf{S}} \psi_j, \quad j = 1, \dots, r_v, \quad (2.2)$$

of which the first three are shown in Fig. 2.1B. A suitable Galerkin model reduction operator,

$$\mathbf{V}_v^\Gamma \in \mathbb{R}^{n_v \times (r_v + n_v^Q)}, \quad (2.3)$$

then needs to be defined, with  $n_v^Q$  as the size of the space of bulk (non-boundary) velocities. In Eq. (2.3), POD modes Eq. (2.2) have to be incorporated such that

velocity degrees of freedom on  $\Gamma_0^{f-\tilde{s}}$  are confined to the lower-dimensional subspace, but those associated to the bulk domain remain unconstrained Hirschvogel et al. (2024). Furthermore, the POD space is decomposed with a partition of unity approach such that each region can exhibit independent kinematics, cf. Fig. 2.1C.

### Strong form problem statement

Here, we briefly state the strong problem of FrSI—fluid dynamics in an ALE reference frame Donea et al. (1982); Duarte et al. (2004) with a reduced structural wall model—subject to non-local flux-dependent tractions at the in- and outflows. The boundary subspace projection is then performed on the discrete system presented in a later section.

The incompressible non-conservative ALE Navier-Stokes equations, defining the conservation of linear momentum and mass over the domain  $\mathcal{Q}$  is written as:

$$\rho \left( \frac{\partial \mathbf{v}}{\partial t} \Big|_{\mathbf{x}_0} + \nabla \mathbf{v}(\mathbf{v} - \mathbf{w}) \right) = \nabla \cdot \boldsymbol{\sigma} \quad \text{in } \mathcal{Q} \times [0, T], \quad (2.4)$$

$$\nabla \cdot \mathbf{v} = 0 \quad \text{in } \mathcal{Q} \times [0, T], \quad (2.5)$$

where  $\nabla$  is the gradient operator with respect to physical space ( $\nabla \mathbf{v} := \frac{\partial v_i}{\partial x_j} \mathbf{e}_i \otimes \mathbf{e}_j$ ) and  $\frac{\partial(\bullet)}{\partial t} \Big|_{\mathbf{x}_0}$  the time derivative in the ALE frame. Further,  $\mathbf{v}$  and  $p$  are the fluid's velocity and pressure,  $\mathbf{w}$  is the ALE domain velocity, and  $\rho = 1.025 \cdot 10^{-6} \frac{\text{kg}}{\text{mm}^3}$  the blood density. The ventricular blood is assumed to be a Newtonian fluid, making the Cauchy stress  $\boldsymbol{\sigma} = -p \mathbf{I} + \mu (\nabla \mathbf{v} + (\nabla \mathbf{v})^T)$ , with the dynamic viscosity  $\mu = 4 \cdot 10^{-6} \text{ kPa} \cdot \text{s}$ . The fluid's boundary wall  $\Gamma_0^{f-\tilde{s}}$  is assumed deformable and is described by a reduced solid mechanics model governed by the balance of linear momentum of finite strain elastodynamics, which entails the physics component of the FrSI method Hirschvogel et al. (2024). Since the displacement field at the boundary can be entirely derived from the fluid's velocity field, kinematic compatibility and continuity of tractions are readily fulfilled by incorporating the following boundary traction, cf. comparable derivations for small strain solid wall models Colciago et al. (2014):

$$\mathbf{t}_0^{f-\tilde{s}} = -h_0 \left( \rho_{0,s} \frac{\partial \mathbf{v}}{\partial t} - \tilde{\nabla}_0 \cdot \tilde{\mathbf{P}} \right) \quad \text{on } \Gamma_0^{f-\tilde{s}} \times [0, T], \quad (2.6)$$

where  $\tilde{\nabla}_0$  is a Nabla operator with respect to the reference frame (considering only in-plane derivatives),  $h_0$  a wall thickness parameter (here 10 mm for ventricle, 5 mm for atrium, and 1 mm for aortic arch),  $\rho_{0,s} = 10^{-6} \frac{\text{kg}}{\text{mm}^3}$  the reduced solid's density, and  $\tilde{\mathbf{P}} = \tilde{\mathbf{P}}(\mathbf{u}_f(\mathbf{v}) + \mathbf{u}_{pre}, \mathbf{v})$  the first Piola-Kirchhoff stress—a general function of the fluid velocity and the fluid displacement at the boundary:

$$\mathbf{u}_f(v) = \int_0^t v \, d\bar{t}. \quad (2.7)$$

The first Piola-Kirchhoff stress is mapped from its material counterpart, the second Piola-Kirchhoff stress,  $\tilde{\mathbf{P}} = (\mathbf{F}_f - \mathbf{F}_f \mathbf{n}_0 \otimes \mathbf{n}_0) \tilde{\mathbf{S}}$ , with the fluid deformation gradient  $\mathbf{F}_f = \mathbf{I} + \nabla_0 \mathbf{u}_f$ , using Eq. (2.7). By eliminating its normal components and re-defining the out-of-plane stretch on assumptions of incompressibility, a membrane right Cauchy-Green tensor,  $\tilde{\mathbf{C}}$ , for the surface as well as its time derivative can be defined. Finally,  $\mathbf{u}_{pre}$  is a prestress displacement computed by methods described in Schein and Gee (2021); Gee et al. (2010). More details on the kinematics and prestress for FrSI can be found in Hirschvogel et al. (2024). The constitutive equation for the reduced solid second Piola-Kirchhoff stress is

$$\tilde{\mathbf{S}} = 2 \frac{\partial \Psi(\tilde{\mathbf{C}})}{\partial \tilde{\mathbf{C}}} + 2 \frac{\partial \Psi_v(\dot{\tilde{\mathbf{C}}})}{\partial \dot{\tilde{\mathbf{C}}}} + \tau_a(t) \mathbf{A}_0, \quad (2.8)$$

with a structural tensor  $\mathbf{A}_0 = \mathbf{I}$  for the atrium (isotropic active stress),  $\mathbf{A}_0 = \tilde{\mathbf{M}}_0$  for the ventricle (active stress in directions of a reduced structural tensor Hirschvogel et al. (2024)), or  $\mathbf{A}_0 = \mathbf{0}$  for the aortic arch (no active stress). The active stress  $\tau_a(t)$  follows the solution of an evolution equation, cf. Hirschvogel et al. (2017). The passive elastic model is of isotropic-exponential type<sup>1</sup> Demiray (1972), and a typical viscous pseudo-potential is used Chapelle et al. (2012).

The coupling to the circulatory system is expressed via  $n_{0d}^b = 7$  non-local constraints, enforcing consistency between the flux over the 3D-0D boundary  $\Gamma_i^{f-0d}$  and the flux variable  $q_i^{0d}$  from the 0D model:

$$\int_{\Gamma_i^{f-0d}} (\mathbf{v} - \hat{\mathbf{w}}) \cdot \mathbf{n} \, dA = \alpha_i q_i^{0d} (\{\Lambda\}_{n_{0d}^b}) \quad \text{in } [0, T]. \quad (2.9)$$

Therein,  $\mathbf{n}$  is a unit outward normal of the current frame, and scaling parameters,  $\alpha_i$ , account for the directionality of flow, i.e. should take the value of  $-1$  if a 0D flux variable is imposed as an inflow to the fluid domain, and  $1$  otherwise. The multipliers  $\{\Lambda\}_{n_{0d}^b}$  impose normal tractions (pressure loads) on their respective in-/outflow boundaries:

$$\mathbf{t}_i^{f-0d} = -\Lambda_i \mathbf{n} \quad \text{on } \Gamma_i^{f-0d} \times [0, T]. \quad (2.10)$$

---

<sup>1</sup> While the myocardium typically exhibits highly anisotropic passive properties Holzapfel and Ogden (2009), it remains inconclusive how its transmurally varying fiber, sheet, and sheet-normal architecture—governing its anisotropic stiffness—can be consistently homogenized throughout the wall and mapped to a 2D surface representation. Since our focus primarily addresses adaptive fluid motion, we prefer an isotropic 2D model whose parameters easily can be calibrated to observed (diastolic) pressure-volume data.

The deformability of the fluid domain here is described by a pseudo-solid's displacement field  $\mathbf{d}$  governed by

$$\nabla_0 \cdot \boldsymbol{\sigma}_g = \mathbf{0} \quad \text{in } \Omega_0 \times [0, T], \quad (2.11)$$

$$\mathbf{d} = \mathbf{u}_f(\mathbf{v}) \quad \text{on } \Gamma_0^{f-s} \times [0, T], \quad (2.12)$$

subject to the essential boundary condition on  $\Gamma_0^{f-s}$ , requiring  $\mathbf{d}$  to take the value of the fluid displacement Eq. (2.7). Here, we use a fully nonlinear ALE model of coupled Neo-Hookean type Holzapfel (2000), which, on the discrete space, is scaled by the inverse of the reference cell's Jacobian determinant Shamanskiy and Simeon (2021). This scaling allows allocating stiffness to more anisotropic boundary elements and have the more regularly shaped bulk elements bear most of the deformation. The ALE deformation gradient and its determinant—as well as the grid/ALE convective velocity in Eq. (2.4)—are given by

$$\widehat{\mathbf{F}} = \mathbf{I} + \nabla_0 \mathbf{d}, \quad \widehat{J} = \det \widehat{\mathbf{F}}, \quad \text{and} \quad \widehat{\mathbf{w}} = \frac{\partial \mathbf{d}}{\partial t}. \quad (2.13)$$

### Weak form and linearization

In the following, we define the continuous weak forms of the strong problem statements suitable for a monolithic finite element implementation in FEniCSx. For this purpose, all integrals are formulated over the respective reference domains, and all gradient operators relate to the undeformed configuration  $\Omega_0$ . The general weak problem can be stated as follows:

Find fluid velocity  $\mathbf{v}$ , pressure  $p$ , multiplier variables  $\{\Lambda\}_{n_{0d}^b}$ , and ALE domain displacements  $\mathbf{d}$  such that conservation of linear momentum,

$$\begin{aligned} R_{\delta v} (\mathbf{v}, p, \{\Lambda\}_{n_{0d}^b}, \mathbf{d}; \delta \mathbf{v}) := & \int_{\Omega_0} \widehat{J} \rho \left( \frac{\partial \mathbf{v}}{\partial t} \Big|_{x_0} + (\nabla_0 \mathbf{v} \widehat{\mathbf{F}}^{-1}) (\mathbf{v} - \widehat{\mathbf{w}}) \right) \cdot \delta \mathbf{v} \, dV_0 \\ & + \int_{\Omega_0} \widehat{J} \boldsymbol{\sigma}(\mathbf{v}, p, \mathbf{d}) : \nabla_0 \delta \mathbf{v} \widehat{\mathbf{F}}^{-1} \, dV_0 + \sum_{i=1}^{n_{0d}^b} \Lambda_i \int_{\Gamma_{0,i}^{f-0d}} \widehat{J} \widehat{\mathbf{F}}^{-T} \mathbf{n}_0 \cdot \delta \mathbf{v} \, dA_0 \\ & + \int_{\Gamma_0^{f-s}} h_0 \left( \rho_{0,s} \frac{\partial \mathbf{v}}{\partial t} \cdot \delta \mathbf{v} + \tilde{\mathbf{P}}(\mathbf{u}_f(\mathbf{v}) + \mathbf{u}_{pre}, \mathbf{v}) : \tilde{\nabla}_0 \delta \mathbf{v} \right) \, dA_0 \\ & + R_{\delta v}^R(\mathbf{v}, \mathbf{d}; \delta \mathbf{v}) + S_{\delta v}^D(\mathbf{v}, p, \mathbf{d}; \delta \mathbf{v}) + S_{\delta v}^{\text{out}}(\mathbf{v}, \mathbf{d}; \delta \mathbf{v}) = 0, \end{aligned} \quad (2.14)$$

conservation of mass,

$$R_{\delta p}(\mathbf{v}, \mathbf{d}; \delta p) := \int_{\Omega_0} \widehat{\mathbf{J}} \nabla_0 \mathbf{v} : \widehat{\mathbf{F}}^{-T} \delta p \, dV_0 + S_{\delta p}^D(\mathbf{v}, p, \mathbf{d}; \delta p) = 0, \quad (2.15)$$

constraints enforcing consistency between 0D and 3D models,

$$\begin{aligned} R_{\delta A} \left( \mathbf{v}, \{\Lambda\}_{n_{0d}^b}, \mathbf{d}; \{\delta \Lambda\}_{n_{0d}^b} \right) := \\ \sum_{i=1}^{n_{0d}^b} \left( \int_{\Gamma_{0,i}^{f,0d}} (\mathbf{v} - \widehat{\mathbf{w}}) \cdot \widehat{\mathbf{J}} \widehat{\mathbf{F}}^{-T} \mathbf{n}_0 \, dA_0 - \alpha_i q_i^{0d} \left( \{\Lambda\}_{n_{0d}^b} \right) \right) \delta \Lambda_i = 0, \end{aligned} \quad (2.16)$$

as well as ALE domain motion,

$$R_{\delta d}(\mathbf{d}, \mathbf{v}; \delta \mathbf{d}) := \int_{\Omega_0} \boldsymbol{\sigma}_g(\mathbf{d}) : \nabla_0 \delta \mathbf{d} \, dV_0 = 0, \quad (2.17)$$

hold true, for all fluid velocity and pressure test functions  $(\delta \mathbf{v}, \delta p)$ , ALE domain motion test functions  $(\delta \mathbf{d})$ , as well as multiplier test functions  $(\{\delta \Lambda\}_{n_{0d}^b})$ . The ALE problem is further subject to the essential boundary condition Eq. (2.12) at the deformable interface where the reduced solid is defined. The constitutive equation for the Cauchy stress is written with respect to the reference frame,  $\boldsymbol{\sigma}(\mathbf{v}, p, \mathbf{d}) = -p \mathbf{I} + \mu \left( \nabla_0 \mathbf{v} \widehat{\mathbf{F}}^{-1} + \widehat{\mathbf{F}}^{-T} (\nabla_0 \mathbf{v})^T \right)$ . In Eq. (2.14),  $R_{\delta v}^R(\mathbf{v}, \mathbf{d}; \delta \mathbf{v})$  is a Robin term used to impose pressure jump-dependent tractions at the mitral and aortic valve planes. This represents a particular challenge, since effects of the mitral and aortic valves need pressure discontinuities across the interfaces of atrium and ventricle as well as ventricle and aortic root. For this purpose, very recently introduced *mixed-dimensional* functionality of FEniCSx is leveraged. This allows to create sub-discretizations (of equal or lower dimension) and make use of functions defined on different but related meshes within one finite element form. Here, the function space for the fluid pressure is defined on each sub-mesh (atrium, ventricle, aorta), and hence is allowed to jump across their respective interfaces. More details on the valve models can be found in Hirschvogel et al. (2025). Furthermore, the terms  $S_{\delta v}^D(\mathbf{v}, p, \mathbf{d}; \delta \mathbf{v})$  in Eq. (2.14) and  $S_{\delta p}^D(\mathbf{v}, p, \mathbf{d}; \delta p)$  in Eq. (2.15) refer to stabilization operators suitable for first-order approximations of both fluid velocity and pressure. Here, we make use of a variant of the G2 stabilization method Johnson (1998); Hoffman and Johnson (2003); Hessenthaler et al. (2017). Furthermore, to prevent backflow-induced divergence, all Neumann/3D-0D coupling boundaries are subject to an outflow stabilization Moghadam et al. (2011), referred to by the term  $S_{\delta v}^{out}(\mathbf{v}, \mathbf{d}; \delta \mathbf{v})$  in Eq. (2.14).

Flux variables  $q_j^{0d} = \mathbf{y} \cdot \mathbf{e}_j$  in Eq. (2.16) are, in general, solutions to a set of  $n_{0d}^e$  0D algebraic and first-order ordinary differential equations in time, with the vector of state variables  $\mathbf{y}$  and  $\mathbf{e}_j$  as the  $j$ -th  $n_{0d}^e$ -dimensional unit vector. We may state the 0D problem as follows: Find 0D model variables  $\mathbf{y}$  such that

$$R_{0d} \left( \mathbf{y}, \{\boldsymbol{\Lambda}\}_{n_{0d}^b}; \delta \mathbf{y} \right) := \left( \dot{\mathbf{g}}(\mathbf{y}, \{\boldsymbol{\Lambda}\}_{n_{0d}^b}) + \mathbf{f}(\mathbf{y}, \{\boldsymbol{\Lambda}\}_{n_{0d}^b}) \right) \cdot \delta \mathbf{y} = 0, \quad (2.18)$$

for all  $\delta \mathbf{y}$ , where  $\mathbf{g}$  is a linear (“left-hand side”) and  $\mathbf{f}$  a possibly nonlinear (“right-hand side”) function in the variable vector  $\mathbf{y}$  and/or multipliers  $\{\boldsymbol{\Lambda}\}_{n_{0d}^b}$ .

The linearizations of the weak forms Eq. (2.14)–(2.17), being the derivatives in the direction of the velocity, pressure, multiplier, and domain displacement trial functions  $\Delta \mathbf{v}$ ,  $\Delta p$ ,  $\{\Delta \boldsymbol{\Lambda}\}_{n_{0d}^b}$ , and  $\Delta \mathbf{d}$ , respectively,

$$K_{\delta(\cdot)_i \Delta(\cdot)_j} := D_{\Delta(\bullet)_j} [R_{\delta(\cdot)_i}], \quad (2.19)$$

are computed using symbolic automatic differentiation in FEniCSx, where  $D_{\Delta(\bullet)_j}$  is the Gâteaux operator with respect to the trial function  $\Delta(\bullet)_j$ . Due to the Dirichlet conditions on the ALE problem, a special consideration is needed for the derivative of the ALE residual with respect to the fluid velocity. Due to the nature of how Dirichlet conditions are applied in FEniCSx, this is taken care of post-discretization.

## Discretization and solution

The problem is discretized with finite elements of piecewise linear Lagrange polynomials in space and a single-step implicit finite difference scheme in time (One-step- $\theta$  scheme, with  $\theta \in ]0; 1]$ ). The projection-based component of the FrSI method requires the reduced solid boundary to be projected to a lower-dimensional subspace spanned by POD modes, cf. Fig. 2.1B depicting the first three modes of this space. This is done by the boundary Galerkin projection operator Eq. (2.3). At the discrete assembled stage, at the current time-step indexed by  $n+1$ , we seek to find the discrete velocity  $\mathbf{v}_{n+1}$ , pressure  $\mathbf{p}_{n+1}$ , 3D-0D coupling multipliers  $\boldsymbol{\Lambda}_{n+1}$ , and domain displacements  $\mathbf{d}_{n+1}$  satisfying

$$\mathbf{r}_{n+1} = \begin{bmatrix} \mathbf{V}_v^T \mathbf{r}_v(\mathbf{V}_v^T \tilde{\mathbf{v}}, \mathbf{p}, \boldsymbol{\Lambda}, \mathbf{d}) \\ \mathbf{r}_p(\mathbf{p}, \mathbf{V}_v^T \tilde{\mathbf{v}}, \mathbf{d}) \\ \mathbf{r}_{\boldsymbol{\Lambda}}(\boldsymbol{\Lambda}, \mathbf{V}_v^T \tilde{\mathbf{v}}, \mathbf{d}) \\ \mathbf{r}_d(\mathbf{d}, \mathbf{V}_v^T \tilde{\mathbf{v}}) \end{bmatrix}_{n+1} = \mathbf{0}, \quad (2.20)$$

where  $\mathbf{r}_v$ ,  $\mathbf{r}_p$ ,  $\mathbf{r}_{\boldsymbol{\Lambda}}$ , and  $\mathbf{r}_d$  are the assembled discrete counterparts of Eq. (2.14)–(2.17), respectively. The trial space projection is  $\mathbf{v} = \mathbf{V}_v^T \tilde{\mathbf{v}}$ , where  $\tilde{\mathbf{v}}$  is the (partly) reduced-dimensional velocity vector. In order to solve Eq. (2.20), a monolithic Newton scheme is employed, resulting in the linearized system of equations to solve for the variable increments in each nonlinear iteration indexed by  $k+1$ :

$$\begin{bmatrix} \mathbf{V}_v^T \mathbf{K}_{vv} \mathbf{V}_v^T & \mathbf{V}_v^T \mathbf{K}_{vp} & \mathbf{V}_v^T \mathbf{K}_{vA} & \mathbf{V}_v^T \mathbf{K}_{vd} \\ \mathbf{K}_{pv} \mathbf{V}_v^T & \mathbf{K}_{pp} & \mathbf{0} & \mathbf{K}_{pd} \\ \mathbf{K}_{Av} \mathbf{V}_v^T & \mathbf{0} & \mathbf{K}_{AA} & \mathbf{K}_{Ad} \\ \mathbf{K}_{dv} \mathbf{V}_v^T & \mathbf{0} & \mathbf{0} & \mathbf{K}_{dd} \end{bmatrix}_{n+1}^k \begin{bmatrix} \Delta \tilde{\mathbf{v}} \\ \Delta \mathbf{p} \\ \Delta \mathbf{A} \\ \Delta \mathbf{d} \end{bmatrix}_{n+1}^{k+1} = - \begin{bmatrix} \mathbf{V}_v^T \mathbf{r}_v \\ \mathbf{r}_p \\ \mathbf{r}_A \\ \mathbf{r}_d \end{bmatrix}_{n+1}^k, \quad (2.21)$$

where sub-block matrices  $\mathbf{K}_{ij}$  are obtained from the assembled discrete counterparts of Eq. (2.19), i.e. the derivatives of the residuals in the direction of the trial functions. Due to the lifting of Dirichlet conditions—ALE domain displacements prescribed to equal the fluid displacements on  $I_0^{f-s}$ , cf. Eq. (2.12)—special considerations have to be carried out to assemble  $\mathbf{K}_{dv}$ . This matrix yields

$$\mathbf{K}_{dv} = \gamma [(\mathbf{I} - \mathbf{I}_f) \mathbf{K}_{dd} \mathbf{I}_f - \mathbf{I}_f], \quad (2.22)$$

where  $\gamma$  is a time-integration factor stemming from the derivative of the fluid displacement with respect to the velocity, and  $\mathbf{I}_f$  is a rank-deficient identity matrix with entries only at indices relating to boundary degrees of freedom of  $I_0^{f-s}$ .

Within one global Newton iteration, prior to solving Eq. (2.21), nonlinear sub-iterations (indexed by  $l$ ) are carried out to find an equilibrium 0D flux (given the current nonlinear iterate  $\mathbf{A}_{n+1}^k$ ) solving the time-discrete version of Eq. (2.18), meaning repeated solves of the linearized 0D model system,

$$\mathbf{K}_{n+1}^{0d,k,l} \Delta \mathbf{y}_{n+1}^{k,l+1} = -\mathbf{r}_{n+1}^{0d,k,l}, \quad (2.23)$$

followed by the solution of Eq. (2.21). In Eq. (2.23),  $\mathbf{K}^{0d}$  is computed with symbolic differentiation using SymPy Meurer et al. (2017).

## Results

Figure 2.2 shows the results of a full heart cycle simulation. The physical time of the simulation is  $T = 1$  s, and a time step size of  $\Delta t = 0.00125$  s was used, hence  $N = 800$  time steps were done. The mid-point single step time-integration method was set to Backward Euler, hence  $\theta = 1$ . The 3D computational domain consists of 265 722 nodes (1 487 039 finite elements), and the overall problem size is 1 790 303 degrees of freedom. The resulting linear system Eq. (2.21) was solved with a FGMRES Saad (1993) algorithm, preconditioned by our recently proposed BGS-S3×3 preconditioner Hirschvogel et al. (2025). All methods are implemented in the open-source FEniCSx- Baratta et al. (2023) and PETSc-based Balay et al. (2022) solver Ambit Hirschvogel (2024).

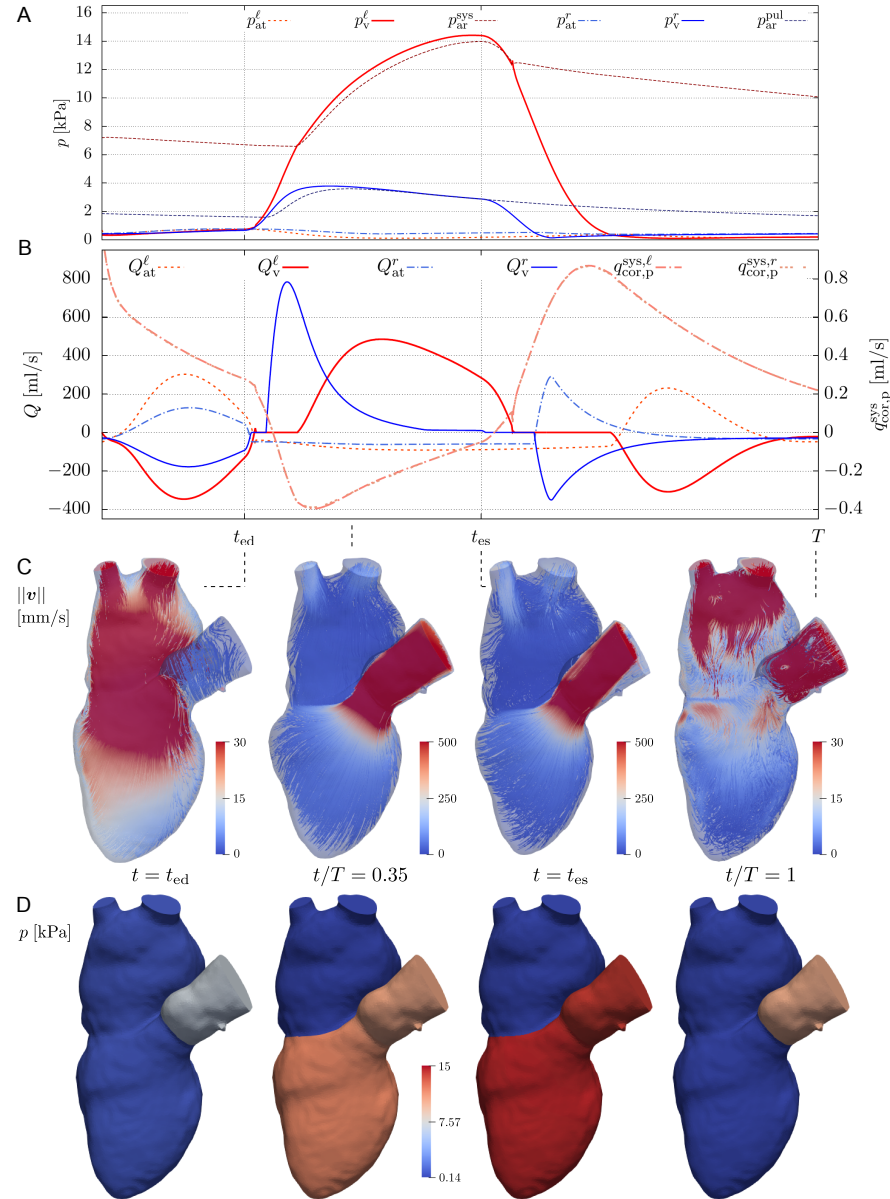


Fig. 2.2: Adapted from Hirschvogel et al. (2025): **A.** Left atrial, left ventricular, systemic arterial, right atrial, right ventricular, and pulmonary arterial pressures over time. **B.** Left atrial, left ventricular, right atrial, right ventricular, left and right proximal coronary fluxes over time. **C.** Magnitude of fluid velocity  $v$ , streamlines on longitudinal cut through deformed domain  $\Omega$ . Note the different scales for diastolic and systolic snapshots. **D.** Fluid pressure  $p$ , plotted on undeformed reference domain  $\tilde{\Omega}_0$ .

## Conclusion

We presented the fluid-reduced-solid interaction (FrSI) method for a patient-specific, large-scale, left heart model, with a focus on a monolithic implementation in a FEniCSx software environment. The model can represent physiologic quantities throughout a heart cycle, and may be used to predict hemodynamics under varying cardiovascular conditions, e.g. for mitral valve regurgitation and repair.

## Software and data availability

The presented results all are computed using Ambit Hirschvogel (2024) release version 1.3, cf. <https://github.com/marchirschvogel/ambit>. All data needed to run the model—the Ambit code as well as a medium (rf1) and fine discretization (rf2, used for generating the results presented), as well as the Ambit input file—are published at <https://zenodo.org/records/14631793>. Running Ambit requires FEniCSx to be installed (installation instructions at <https://github.com/FEniCS/dolfinx>), specifically the dolfinx development version dating to Git hash 4392bc84f440d7418ec4491a4a827d50720cb7d7 (Nov 28, 2024). The model might as well run with newer dolfinx versions, however it is not tested.

**Acknowledgements** DN acknowledges funding from the Engineering and Physical Sciences Research Council Healthcare Technology Challenge Award (EP/R003866/1), and support from the Wellcome Trust EPSRC Centre of Excellence in Medical Engineering (WT 088641/Z/09/Z) and the NIHR Biomedical Research Centre at Guy's and St. Thomas' NHS Foundation Trust and KCL.

## References

- Alnæs MS, Blechta J, Hake JE, Johansson A, Kehlet B, Logg A, Richardson C, Ring J, Rognes ME, Wells GN (2015) The FEniCS project version 1.5. Archive of Numerical Software 3
- Arthurs CJ, Lau KD, Asrress KN, Redwood SR, Figueroa CA (2016) A mathematical model of coronary blood flow control: simulation of patient-specific three-dimensional hemodynamics during exercise. Am J Physiol Heart Circ Physiol 310(9):H1242–H1258, doi:10.1152/ajpheart.00517.2015
- Balay S, Abhyankar S, Adams MF, Benson S, Brown J, Brune P, Buschelman K, Constantinescu E, Dalcin L, Dener A, Eijkhout V, Gropp WD, Hapla V, Isaac T, Jolivet P, Karpeev D, Kaushik D, Knepley MG, Kong F, Kruger S, May DA, McInnes LC, Mills RT, Mitchell L, Munson T, Roman JE, Rupp K, Sanan P, Sarich J, Smith BF, Zampini S, Zhang H, Zhang H, Zhang J (2022) PETSc/TAO users manual. Tech. Rep. ANL-21/39 - Revision 3.17, Argonne National Laboratory
- Baratta IA, Dean JP, Dokken JS, Habera M, Hale JS, Richardson CN, Rognes ME, Scroggs MW, Sime N, Wells GN (2023) DOLFINx: The next generation FEniCS problem solving environment. doi:10.5281/zenodo.10447666, URL <https://doi.org/10.5281/zenodo.10447666>

- Bonini M, Hirschvogel M, Ahmed Y, Xu H, Young A, Tang PC, Nordsletten D (2022) Hemodynamic modeling for mitral regurgitation. *The Journal of Heart and Lung Transplantation* 41(4 (Supplement)):S218–S219, doi:10.1016/j.healun.2022.01.1685
- Chapelle D, Tallec PL, Moireau P, Sorine M (2012) Energy-preserving muscle tissue model: formulation and compatible discretizations. *Journal for Multiscale Computational Engineering* 10(2):189–211, doi:10.1615/IntJMultCompEng.2011002360
- Colciago CM, Deparis S, Quarteroni A (2014) Comparisons between reduced order models and full 3D models for fluid-structure interaction problems in haemodynamics. *Journal of Computational and Applied Mathematics* 265:120–138, doi:10.1016/j.cam.2013.09.049
- Demiray H (1972) A note on the elasticity of soft biological tissues. *Journal of Biomechanics* 5(3):309–311, doi:10.1016/0021-9290(72)90047-4
- Donea J, Giuliani S, Halleux J (1982) An arbitrary Lagrangian-Eulerian finite element method for transient dynamic fluid-structure interactions. *Computer Methods in Applied Mechanics and Engineering* 33(1–3):689–723, doi:10.1016/0045-7825(82)90128-1
- Duarte F, Gormaz R, Natesan S (2004) Arbitrary Lagrangian-Eulerian method for Navier-Stokes equations with moving boundaries. *Computer Methods in Applied Mechanics and Engineering* 193(45–47):4819–4836, doi:10.1016/j.cma.2004.05.003
- Garcia-Villalba M, Rossini L, Gonzalo A, Vigneault D, Martinez-Legazpi P, Durán E, Flores O, Bermejo J, McVeigh E, Kahn AM, Álamo JC (2021) Demonstration of patient-specific simulations to assess left atrial appendage thrombogenesis risk. *Front Physiol* 12(596596), doi:10.3389/fphys.2021.596596
- Gee MW, Förster C, Wall WA (2010) A computational strategy for prestressing patient-specific biomechanical problems under finite deformation. *International Journal for Numerical Methods in Biomedical Engineering* 26(1):52–72, doi:10.1002/cnm.1236
- Hessenthaler A, Röhrle O, Nordsletten D (2017) Validation of a non-conforming monolithic fluid-structure interaction method using phase-contrast MRI. *Int J Numer Method Biomed Eng* 33(8):e2845, doi:10.1002/cnm.2845
- Hirschvogel M (2024) Ambit – A FEniCS-based cardiovascular multi-physics solver. *Journal of Open Source Software* 9(93):5744, doi:10.21105/joss.05744
- Hirschvogel M, Bassiliou M, Jagschies L, Wildhirt SM, Gee MW (2017) A monolithic 3D-0D coupled closed-loop model of the heart and the vascular system: Experiment-based parameter estimation for patient-specific cardiac mechanics. *Int J Numer Method Biomed Eng* 33(8):e2842, doi:10.1002/cnm.2842
- Hirschvogel M, Balmus M, Bonini M, Nordsletten D (2024) Fluid-reduced-solid interaction (FrSI): Physics- and projection-based model reduction for cardiovascular applications. *Journal of Computational Physics* 506:112921, doi:10.1016/j.jcp.2024.112921, URL <https://www.sciencedirect.com/science/article/pii/S0021999124001700>
- Hirschvogel M, Bonini M, Balmus M, Nordsletten D (2025) Effective block preconditioners for fluid dynamics coupled to reduced models of a non-local nature. *Computer Methods in Applied Mechanics and Engineering* 435:117541, doi:10.1016/j.cma.2024.117541
- Hoffman J, Johnson C (2003) Adaptive Finite Element Methods for Incompressible Fluid Flow, Springer Berlin Heidelberg, Berlin, Heidelberg, pp 97–157. doi:10.1007/978-3-662-05189-4\_3
- Holzapfel GA (2000) Nonlinear Solid Mechanics – A Continuum Approach for Engineering. Wiley Press Chichester
- Holzapfel GA, Ogden RW (2009) Constitutive modelling of passive myocardium: A structurally based framework for material characterization. *Phil Trans R Soc A* 367(1902):3445–3475, doi:10.1098/rsta.2009.0091
- Johnson C (1998) Adaptive finite element methods for conservation laws, Springer Berlin Heidelberg, Berlin, Heidelberg, pp 269–323. doi:10.1007/BFb0096354
- Kikinis R, Pieper SD, Vosburgh KG (2014) 3D Slicer: A Platform for Subject-Specific Image Analysis, Visualization, and Clinical Support, Springer New York, New York, NY, pp 277–289. doi:10.1007/978-1-4614-7657-3\_19

- McCormick M, Nordsletten D, Kay D, Smith N (2011) Modelling left ventricular function under assist device support. International Journal for Numerical Methods in Biomedical Engineering 27(7):1073–1095, doi:10.1002/cnm.1428
- Meurer A, Smith CP, Paprocki M, Čertík O, Kirpichev SB, Rocklin M, Kumar A, Ivanov S, Moore JK, Singh S, Rathnayake T, Vig S, Granger BE, Muller RP, Bonazzi F, Gupta H, Vats S, Johansson F, Pedregosa F, Curry MJ, Terrel AR, Roučka v, Saboo A, Fernando I, Kulal S, Cimrman R, Scopatz A (2017) SymPy: symbolic computing in Python. PeerJ Computer Science 3:e103, doi:10.7717/peerj-cs.103, URL <https://doi.org/10.7717/peerj-cs.103>
- Moghadam ME, Bazilevs Y, Hsia TY, Vignon-Clementel IE, Marsden AL, Modeling of Congenital Hearts Alliance (MOCHA) (2011) A comparison of outlet boundary treatments for prevention of backflow divergence with relevance to blood flow simulations. Computational Mechanics 48(3):277–291, doi:10.1007/s00466-011-0599-0
- Nordsletten DA, McCormick M, Kilner PJ, Hunter P, Kay D, Smith NP (2011) Fluid-solid coupling for the investigation of diastolic and systolic human left ventricular function. International Journal for Numerical Methods in Biomedical Engineering 27(7):1017–1039, doi:10.1002/cnm.1405
- Rathinam M, Petzold LR (2003) A new look at Proper Orthogonal Decomposition. SIAM Journal on Numerical Analysis 41(5):1893–1925, doi:10.1137/S0036142901389049
- Saad Y (1993) A flexible inner-outer preconditioned GMRES algorithm. SIAM J Sci and Stat Comput 14(2):461–469, doi:10.1137/0914028
- Schein A, Gee MW (2021) Greedy maximin distance sampling based model order reduction of prestressed and parametrized abdominal aortic aneurysms. Advanced Modeling and Simulation in Engineering Sciences 8(18), doi:10.1186/s40323-021-00203-7
- Schwarz EL, Pegolotti L, Pfaller MR, Marsden AL (2023) Beyond CFD: Emerging methodologies for predictive simulation in cardiovascular health and disease. Biophys Rev (Melville) 4(1):011301, doi:10.1063/5.0109400
- Shamanskiy A, Simeon B (2021) Mesh moving techniques in fluid-structure interaction: robustness, accumulated distortion and computational efficiency. Computational Mechanics 67:583–600, doi:10.1007/s00466-020-01950-x
- Simmetrix Inc (2023) SimModeler (Version 2023.0) [Computer Software]. URL <http://simmetrix.com>
- Zingaro A, Bucelli M, Fumagalli I, Dede' L, Quarteroni A (2023) Modeling isovolumetric phases in cardiac flows by an Augmented Resistive Immersed Implicit Surface method. International Journal for Numerical Methods in Engineering 39(12):e3767, doi:10.1002/cnm.3767



## Glossary

Use the template *glossary.tex* together with the Springer Nature document class SVMono (monograph-type books) or SVMult (edited books) to style your glossary in the Springer Nature layout.

**glossary term** Write here the description of the glossary term. Write here the description of the glossary term. Write here the description of the glossary term.

**glossary term** Write here the description of the glossary term. Write here the description of the glossary term. Write here the description of the glossary term.

**glossary term** Write here the description of the glossary term. Write here the description of the glossary term. Write here the description of the glossary term.

**glossary term** Write here the description of the glossary term. Write here the description of the glossary term. Write here the description of the glossary term.

**glossary term** Write here the description of the glossary term. Write here the description of the glossary term. Write here the description of the glossary term.



# **Index**

acronyms, list of, xvii

dedication, v

glossary, 17

symbols, list of, xvii